PHYSICAL REVIEW B VOLUME 24, NUMBER 2 15 JULY 1981

Enhancement of surface and volume photoeffects in cesiated Al thin films by controlled excitation of surface plasma waves at low photon energies

G. Hincelin

Conservatoire National des Arts et Metiers, Laboratoire de Physique du Vide, Equipe de Recherche Associée 660, 292 rue Saint Martin, 75141 Paris, France

(Received 22 December 1980)

At photon energies far below the surface-plasmon energy, photoemission from a metal surface may be described in terms of volume and surface photoeffects, whose respective contributions in absolute values are easily calculated with the help of phenomenological models with the condition, however, that several basic parameters have been previously determined experimentally. Aluminum thin films directly evaporated in ultrahigh vacuum onto a prism are smooth enough to exhibit a pure volume effect by illumination with s-polarized radiation, even after activation of their surfaces by a submonolayer of cesium. Surface plasma waves (SPW) excited at the metal-film–vacuum interface by the attenuated-total-reflection method allow an accurate determination of the thickness and of the local dielectric constant of the film before and after Cs deposition, respectively. After the determination of the electron escape length $L(\omega)$ in the photon energy domain $1.5 < \hbar\omega < 4$ eV and measurement of the spectral sensitivities of the film illuminated on its front face with s- and p-polarized light successively, the surface photoemission spectrum is obtained. A careful study of the respective contributions of the volume and surface effects is then carried out, in the presence of SPW excited in the film by illumination through the prism. The surface effect is more greatly enhanced than the volume effect by the SPW fields, and the respective variations of these effects as a function of the incidence angle are very different. At photon energies not too far from the threshold, the surface-effect photoemission far exceeds (even by one order for magnitude) the volume photoemission. Excellent agreement is obtained between measured and calculated values of total photoemission yield.

I. INTRODUCTION

Electron photoemission from a metal surface into vacuum originates from the interaction of electromagnetic radiation with the electrons in the metal. For a perfectly smooth surface the only source of electron photoexcitation is the field of the transmitted wave, as surface plasma waves (SPW) cannot be excited.

Electron photoexcitation, which obeys energy and momentum conservation laws, takes place in essentially two ways, by interacting either with the surface potential barrier or with the lattice potential in the bulk. The nonperiodicity in the direction normal to the solid-vacuum interface has the same function as the lattice periodicity: It causes photoexcitation via optical absorption, and it supplies normal momentum as required during the electron escape process.

Electron photoexcitation in the volume is an important source of photoelectrons and photoemission from the bulk may be described by the familiar "three-step model,"[1-4] in which optical excitation, transport of the electron to the surface, and escape of this electron through the potential barrier may be treated as separate steps. This model, which has the invaluable advantage of easily allowing quantitative calculations, may be considered as physically correct if the mean free path of the excited electrons is very large compared to the lattice constant,[5,6] a condition that always holds when low-energy photons are used.

The three-step model necessitates the simplifying assumption that photoexcitation is an isotropic phenomenon (i.e., independent of the relative orientation of the wave electric field vector and the lattice vectors). This point has been discussed in detail in the case of polycrystalline metals,[7,8] and it seems that at photon energies very low compared to the surface plasmon energy ($\hbar\omega_{sp}$) photoexcitation in the bulk may be considered as isotropic.

Photoemission from the bulk (volume effect) may be calculated by using the classical Fresnel formulas which allow the determination of the optical energy density absorbed in the solid as a function of the metal dielectric constant $\epsilon(\omega) = \epsilon'(\omega) + j\epsilon''(\omega)$.[9,10] For a free-electron-like metal, $\epsilon(\omega)$ may be represented by an analytical formula, but in real metals interband transitions are responsible for a supplementary term. This term cannot be calculated with precision, and it is better to use in the calculations the experimental values of $\epsilon(\omega)$. We shall, however, emphasize that such a macroscopic theory based on local values of the dielectric function may be used only if the perturbation due to the surface extends to a depth very small compared to the wavelength of the incident radiation. This is true at low photon energies but in the domain of the volume plasmon frequency and with a p-polarized wave, Fresnel's formulas are no longer valid for calculating with good accuracy the electromagnetic field in the vicinity of the surface. On the other hand, the

local approximation is always valid for s-polarized radiation, and a local $\epsilon(\omega)$ may then be used for all photon energies.

The surface photoexcitation process is at the origin of the "surface photoelectric effect," which was historically the first mechanism suggested for explaining the photoelectric effect.[11] Owing to its one-dimensional character, the potential barrier can only act if the incident radiation has an electric field component normal to the surface. Therefore the surface effect is limited to p-polarized light excitation at non-normal incidence, at least for ideally smooth surfaces. This effect strongly depends on the electric field distribution in the surface region.

In local theories the surface is considered only as a geometrical discontinuity between two homogeneous media having different dielectric constants. Field calculation at the metal surface is based on the assumption of an infinitely thin surface layer containing an infinite density of electric charge, responsible for the discontinuity of the normal electric field component when crossing the surface. As a matter of fact, charge density and potential vary very rapidly but continuously through the surface, in a region of 1–2 angströms in thickness.

For this reason, local theories can be used to calculate surface photoemission only if the perturbation due to the incident p-polarized wave remains localized in this surface transition region. This will be the case for photon energies far below the volume plasmon energy $\hbar\omega_p$. On the contrary, around and above $\hbar\omega_p$, the charge density may be profoundly modified by the incident radiation in a thick surface layer, and a nonlocal theory should be necessary to interpret correctly both optical and photoelectric phenomena.

A theory of the surface effect accounting for the variations of the surface polarization charge density by p-polarized radiation has been elaborated by Endriz[12] for Al, a nearly-free-electron metal. The surface effect is considered as originating from the interaction of electrons with the induced charge-density variations. The behavior of the surface charge has a fundamental influence on the energy dependence of the surface effect: Numerical evaluation of the characteristic excitation factors indicates an enhancement in the surface effect at energies well below $\hbar\omega_p$, and, for energies near $\hbar\omega_p$, surface charge screening of the excitation fields leads to a total suppression of the surface effect. Another significant result of Endriz's work is that surface plasma waves may be considered as a particular p-polarized light excitation under appropriate complex angles of incidence. But the direct surface effect will be sufficiently strong at energies near threshold to dominate the photoemission associated with the decay of surface plasmons which could be excited on a real surface by coupling through small surface roughness.[8]

More recently a calculation has been performed that uses an improved surface potential barrier and treats the spatial behavior of the photoexcitation by the electromagnetic field in a self-consistent way.[13] The calculated surface photoyields (in electrons per absorbed photon) do not differ appreciably from those calculated by Endriz.

A possibility for determining the total photoyield (surface plus volume effects) consists in considering that photoemission may be viewed as a one-step process, and a number of authors have derived the photocurrent from the global interaction of the electromagnetic field with a solid.[14–16] These theories lead to formulations of high complexity without distinction of volume and surface effects. To our knowledge they have never been used to calculate real values of photoemission yields.

Finally, another way to describe the physical action of a p-polarized radiation on the electrons of a metal has been explored by Kliewer,[17,18] using a nonlocal description of the dielectric response of the metal to an external electromagnetic perturbation. It is then possible to show that besides the classical transverse wave, an infinite number of longitudinal polarization waves are excited in the metal, whose electric field adds to the field of the transmitted transverse wave.[19] These longitudinal waves are strongly damped and localized in a thin layer near the surface. The wave-electron interaction is described through a transverse dielectric constant ϵ_t and a longitudinal dielectric constant ϵ_L. In addition, for the light incident upon the electron gas from vacuum, the electric field component E_z normal to the surface is continuous across the surface.

The dielectric constants ϵ_t and ϵ_L are functions of ω and the wave vector q. In a real metal a useful approximation may be to treat the free electrons nonlocally and the bound electrons locally. But in these conditions the continuity of E_z across the surface no longer exists. Kliewer[18] gives the expressions for $\epsilon_t(\omega, q)$ and $\epsilon_L(\omega, q)$ and calculates total photoyields for Al for various photon energies as functions of the incidence angle and of the electron escape length. The nonlocal theory of Kliewer has been applied in a simplified form by Chabrier *et al.*[20,21] in order to interpret quantitatively experimental results obtained with Ag thin films. From this work, it may be emphasized that, at low photon energies, the longitudinal polarization waves are strongly damped, and the

total photoemission yield may be considered as the sum of two terms. The first one corresponds to a good approximation, to the classical volume effect essentially due to the transverse wave energy absorbed in the bulk, which may be calculated by using the three-step model and the local dielectric constant $\epsilon(\omega)$. The second would be a surface effect, originating in the absorbed energy associated with the total component of the electric field $E_z(0)$ normal to the surface, existing in the metal at the metal–vacuum interface. The nonlocal theory of Kliewer in its simplified form allows a correct description of the variations of the surface photoyield as a function of the photon energy, even in the critical energy domain of the surface and volume plasmons, but is unable to furnish values of the photoyield in good agreement with experiment.

The work that we present in this paper is not a comparison between results given by local and nonlocal theories, but an attempt to calculate quantitative contributions of volume and surface photoeffects to the global photoemission from a metal thin film in which surface plasma waves are excited by the attenuated total reflection (ATR) method.[22,23]

In summary, and in agreement with the conclusions of the Endriz's work,[12] we consider that Al is the best material for obtaining excellent agreement between experimental results and calculations based upon the "old" theory of photoemission, including a three-step model for the volume effect and a phenomenological surface effect. Indeed, Al films having very smooth surfaces may be prepared by vacuum evaporation.[3,24] In addition, the Al surface plasmon energy ($\hbar\omega_{sp} = 10.3$ eV), is very high compared to the work function W_ϕ that can be attained by covering the emitting surface with a very thin layer of Cs ($W_\phi = 1.5$ eV). In these conditions, volume and surface effects may be considered to a good approximation as being two independent effects, and the corresponding photoyields can be calculated by using simple phenomenological models, (i) a three-step model with isotropic photoexcitation for the volume effect and (ii) a surface photoyield proportional to the energy associated with the normal component of the electric field on the metal side in the plane of the metal–vacuum interface. A local description for the dielectric constant may be used in both cases, since the longitudinal polarization waves excited by the p-polarized light are concentrated in the surface transition layer, whose thickness is negligible compared to the electron escape depth in the visible and near-ir energy domain.

In order for any theory to furnish accurate values of the total emitted current, preliminary experiments are necessary to determine carefully the thin film dielectric function $\epsilon(\omega)$ and exact thickness, the electron escape length L, and the proportionality factor in the surface effect.

In Sec. II we shall examine briefly the various methods that can be used to couple an external p-polarized radiation to an SPW in a thin film and the conditions required to obtain a pure volume effect with an s-polarized wave. Section III will be devoted to the description of the experimental UHV setup and of the methods used to prepare very smooth Al surfaces by evaporation on a fused silica prism, to control the surface smoothness, and to lower the Al work function with Cs.

The experimental results concerning the reflecting power of the film illuminated through the prism in order to excite SPW, and the photoyields obtained with s- and p-polarized light, when the incident radiation is directed onto the film surface either from the vacuum side (front illumination), or through the prism (rear illumination), are given in Sec. IV. In Sec. V we calculate the complex dielectric constant for the clean and for the cesiated Al surface, and it is shown that the influence of a submonolayer of Cs on the optical properties of Al can be neglected.

The angular variations of the photoyield measured successively with s- and p-polarized light show that photoemission from s-polarized light has its origin in a pure volume effect. Starting from this observation, the escape length of electrons is calculated in the whole energy domain, $1.5 < \hbar\omega < 4$ eV, in Sec. VI, as well as the amplitude of the surface photoeffect, and the proportionality factor between surface photoyield and the surface energy density associated with the normal component of the electric field.

Finally, all useful film parameters being known, Sec. VII reports on the calculation of the respective parts of the volume and surface effects enhanced by excitation of an SPW at the emitting surface. Examples are given for three wavelengths, showing that the relative contribution of surface effect dramatically increases when approaching the emission threshold, and decreases slowly in the uv domain. Angular variations of each photoyield are analyzed in detail.

Excellent agreement is obtained between calculated and experimental absolute values of the total photoyield for all wavelengths, demonstrating *a posteriori* the validity of our preliminary assumptions and of the models used for the calculation.

II. EXCITATION OF SURFACE PLASMA WAVES

Let us consider a semi-infinite metal characterized by its complex permittivity $\epsilon_2 = \epsilon_2' + j\epsilon_2''$ in

contact with a dielectric material of real permittivity ϵ_1. Nonradiative surface plasma waves may be excited at the plane interface by photons of energy $\hbar\omega$ such as $\hbar\omega < \hbar\omega_{sp}$. The frequency upper limit ω_{sp} is given by the condition

$$\epsilon_2'(\omega_{sp}) = -\epsilon_1$$

and for a free-electron-like metal is simply related to the frequency of the volume plasma oscillations by

$$\omega_{sp} = \omega_p(1+\epsilon_1)^{-1/2}.$$

This relation has been experimentally verified quite well for alkali metals and aluminum.[25]

An SPW corresponds to electric charge oscillations at the metal surface, which induce electromagnetic fields. The electric field has a component E_x tangent to the surface and parallel to the direction of propagation of the wave and a component E_z normal to the surface. The amplitudes of the fields decrease exponentially from the surface. The frequency ω and K_{px}, a component of the SPW wave vector K_p, obey a dispersion relation obtained by writing the continuity of K_{px} across the metal-dielectric interface.

The real part of K_{px} being always greater than $K_0 = \omega/v$ (v is the velocity of light in the dielectric material), an SPW cannot be directly excited by a plane monochromatic p-polarized wave obliquely incident on the metal surface through the dielectric because of the impossibility of matching the x components of the wave vectors of both waves. Conversely, an SPW propagating at the metal surface cannot radiate into the adjacent dielectric medium. To excite an SPW at the metal surface, the wave vector component K_{ix} of the incident wave has to be increased, by using either a rough surface, or a special coupling device with an optical index $n > 1$.

Surface roughness may be characterized by a roughness spectrum $g(K_s)$, which is the Fourier transform of the autocorrelation function of the statistically rough surface, and a the rms height variations.[26,27] Momentum-conserving transitions are then possible from an initial incident photon to a final plasmon traveling along the surface with a momentum $\hbar K_{px}$, the following relation being fulfilled:

$$\frac{\omega}{c}\sin\varphi + K_s = K_{px}(\omega).$$

φ is the angle of incidence and $K_s = 2\pi/a_s$, the wave vector associated with the distance a_s separating microreliefs, measured along the surface. The ability of the surface to provide such coupling is roughly proportional to $a^2 g(K_s)$ Ref. 28) and then strongly depends on the shape of the surface-roughness spectrum and on the height of the surface irregularities. For short correlation lengths, $g(K_s)$ will extend to high K_s values ($K_s > \omega/c$), and coupling to surface plasmons will be correspondingly high even for normal incidence ($\varphi = 0$). The same coupling mechanism exists between decaying plasmons and radiated photons, and for a rough surface an SPW can be detected by measuring the light emitted from the surface.

Experiments prove that the coupling efficiency attains its maximum for frequencies near ω_{sp} and the SPW excitation produces an absorption peak on the reflectivity curve $R_p(\omega)$ obtained at nearly normal incidence.[29,30] In these conditions, the optical excitation of an SPW in the visible and ir domain ($1.5 < \hbar\omega < 4$ eV) by roughness will be more difficult with Al ($\hbar\omega_{sp} = 10.3$ eV) than with Ag ($\hbar\omega_{sp} = 3.6$ eV).

The ATR method for controlled optical excitation of surface plasmons has been proposed by Otto[22] and Kretschmann and Raether.[23] A possible configuration of the coupling device is represented in the Fig. 1. A thin metal film is evaporated onto the plane face of a fused silica prism having a real index $n_1 = \epsilon_1^{1/2}$ and illuminated through the prism by plane p-polarized monochromatic light at an incidence angle φ greater than φ_L, the critical angle beyond which total reflection occurs ($n_1 \sin\varphi_L = 1$). The wave-vector component K_{ix} parallel to the surface,

$$K_{ix} = n_1 \frac{\omega}{c}\sin\varphi = n_1 K_0 \sin\varphi,$$

may take values greater than K_0, and by varying φ, may be equal to K_{px}', the real part of K_{px}, for an incidence angle φ_0 such as

$$n_1 K_0 \sin\varphi_0 = K_{px}'.$$

K_{px} is given by the dispersion relation of the SPW at the metal–vacuum interface, calculated for a thin metal film of thickness d, with plane parallel surfaces inserted between two semi-infinite dielectric media of real permittivities $\epsilon_1(\omega)$ and

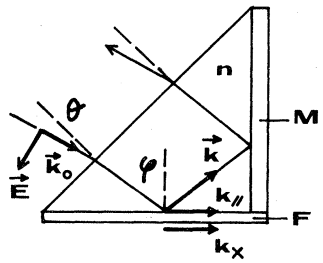

FIG. 1. Illumination of a thin film F through a prism of index n. M is a thick Al mirror. The wave vector K_0 changes into $K = nK_0$.

$\epsilon_3(\omega)=1$, respectively.[22]

With increasing φ, the reflectivity $R_p(\varphi)$ of the prism–metal interface decreases and attains a minimum value R_m at an incident angle $\varphi_0' \sim \varphi_0$. R_m will be close to zero for a correctly chosen value d_0 of the film thickness. Since $\varphi > \varphi_L$, the energy flux transmitted into medium 1 is zero, and the reflectivity decrease must be attributed to a supplementary absorption in the film of the electromagnetic energy due to the excitation of an SPW at the metal–vacuum interface.

However, through the above-mentioned roughness-aided mechanism, a tiny part of the energy can be radiated into medium 1 from the SPW, and for high superficial energy densities, the flux of scattered photons becomes detectable, even for optically good films. The yield of scattered light increases with the rms value of the surface microreliefs, and a measurement of the light flux emitted from the metal surface when SPW are excited allows a fine control of the optical quality of the surface.[31-33] For example, with silver films controlled by reflectometry and showing no visible absorption dip in their $R_p(\omega)$ curve in the vicinity of ω_{sp}, the total scattered light may represent a few 10^{-4} of the incident flux. Recording on an xy plotter the scattered intensity $I_s(\varphi)$ as a function of φ leads to a sharp peak when $\varphi \sim \varphi_0$. For Al films evaporated in a classical high vacuum ($p \simeq 10^{-7}$ Torr) and then examined in air, a small amount (10^{-5} to 10^{-4} in relative value) of scattered light has been observed.[34] As far as we know, no measurement of scattered light from Al films prepared and studied under UHV have been reported to date. We shall see later that for these films the scattered light yield remains beneath 10^{-5}.

Controlled excitation of SPW by the ATR method allows accurate determination of the optical constants and thickness d of the metal film,[35,36] using the simple model represented Fig. 2. The film

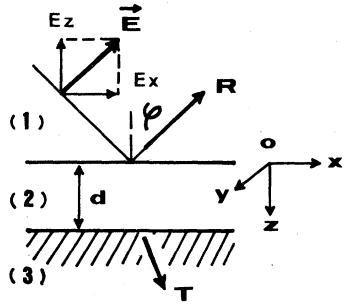

FIG. 2. Coordinate system and photoemitter arrangement: the three-media model. R is the reflectivity; T, the transmission. (1) and (3) are lossless dielectrics, and (2) the metal film of thickness d.

is assumed to be homogeneous with a local dielectric constant $\epsilon_2(\omega)$.

The interface 1-2 (metal–prism) is illuminated by p-polarized radiation at an incidence angle φ. From the Fresnel coefficient r_i of the $i/(i+1)$ interface,

$$r_i = \frac{\epsilon_i K_{i+1} - \epsilon_{i+1} K_i}{\epsilon_i K_{i+1} + \epsilon_{i+1} K_i}, \quad i = 1, 2$$

the reflection coefficient r_{12},

$$r_{12} = \frac{r_1 + r_2 \exp(2jdK_2)}{1 + r_1 r_2 \exp(2jdK_2)},$$

and finally the reflectivity $R_p = |r_{12}|^2$ can be calculated. In the expression giving r_i, K_i is the component of the wave vector normal to the surface in medium i, such as

$$K_i = K_i' + jK_i'' = \frac{\omega}{c}(\epsilon_i - \epsilon_1 \sin^2\varphi)^{1/2}, \quad i = 1, 2, 3.$$

These relations hold for all values of φ, and particularly in the whole angular domain of SPW excitation.

The experimental function $R_p(\varphi)$ depends on three adjustable parameters ϵ_2', ϵ_2'', and d. By adapting the computed reflectance function to the experimental curve, these parameters can be obtained with high accuracy for aluminum films as we shall see later.

III. EXPERIMENTAL SETUP AND MEASUREMENT METHODS

Al thin films are prepared and studied *in situ* in an UHV chamber evacuated by a 400-l/s ion pump and a 2000-l/s titanium getter pump. After a 20-h baking at 300 °C, the limit pressure remains in the range $1-5\times10^{-11}$ Torr. High-purity Al is evaporated from a resistively heated tungsten wire, and cesium, used to lower the Al work function, is vaporized from a Cs dispenser (SAES getters, Milano).

A quartz-crystal thickness monitor measures the final film thickness with an accuracy of ±1 nm. The films are evaporated on a lateral face of a right-angle-fused silica prism supported by a rigid vertical stem which can rotate around its axis. The rotation movement is activated from outside the vacuum tank through a magnetic coupler having no detectable angular shift. Angular orientation of the prism is defined and reproduced within an accuracy domain of ±0.01°.

In photoemission experiments, electrons are collected on a ring-shaped anode kept at a positive potential (+300 V), the emitting film being connected to ground through a picoammeter (Keithley electrometer 610C) allowing current

intensity measurements down to 10^{-14} A. The vacuum chamber and its pumping unit are mounted on a mobile carriage and, after the end of the baking procedure, the whole system is carefully positioned and finally clamped onto a heavy vibration-free table supporting part of the optical system used for illuminating the film and measuring its reflectivity R_p.

The optical layout is schematically represented in Fig. 3. A high-pressure Xe lamp (Osram XBO, 450 W) and a high-dispersion grating monochromator are used to obtain a nearly monochromatic beam of wavelength λ, adjustable from 300 to 1250 nm with a bandwidth of about 1 nm. The divergent beam issuing from the monochromator falls upon a cylindrical mirror M_1, which delivers a beam of rays nearly parallel to the propagation axis with a maximum obliquity less than 3×10^{-4} rad. This rectangular cross-section beam is then polarized by a glan-type prism and enters the vacuum chamber through a fused silica window free of birefringence. After two successive reflections, one from each metallized face of the right-angle prism (one is covered by a thick Al mirror, the other by the evaporated thin Al film), according to an arrangement proposed by Bosenberg,[37] the light beam leaves the chamber through the same window. The angular displacement θ of the prism is referenced to the direction normal to the prism hypotenuse face, itself determined by an autocollimation technique with an accuracy better than 0.01°.

While rotating the prism, the emerging beam remains rigorously parallel to the incident beam. A second cylindrical mirror M_2 compensates the transverse beam displacement accompanying the prism rotation and focuses the light always at the same point on the photocathode of the photomultiplier PM_1, a condition necessary to eliminate the influence of local cathode sensitivity variations on the accuracy in $R_p(\theta)$ measurements. Photoemission current and reflectivity variations are recorded versus θ on an xy double trace recorder. Values of the prism index n_1 are known for all wavelengths, the uncertainty being less than 10^{-4} in relative value, and the real incidence angle φ of the light at the prism–metal interface may be calculated within an accuracy of 0.02°.

A second photomultiplier PM_2 associated with a large diameter metal tube, whose internal polished and silvered wall plays the role of a photon collector, allows the detection of the light possibly scattered from the Al film when SPW are excited. Defining the scattered light yield $D_s = \phi_s/\phi_i$ as the ratio of the total scattered flux to the incident flux intensity, values of D_s as low as 10^{-5} could be detected in the whole range of wavelengths delivered by the monochromator.

It is possible to illuminate the film directly on its vacuum interface at three incidence angles $\varphi^+ = 0°$, 45°, and 70°, respectively. The reflected light beam leaves the chamber through windows, in order to avoid spurious reflections on the inner walls.

The incident radiation flux may be measured accurately for each wavelength in the domain $300 < \lambda < 1000$ nm by introducing in the light path a large-diameter Si photodiode. A Ge photodiode is used for wavelengths greater than 1 μm. Both diodes have been calibrated at the Institut National de Métrologie by comparison with absolute thermoelectric radiometers. The diode surfaces being perpendicular to the beam direction, their spectral sensitivity is assumed to be independent of the light polarization. A silica plate placed in front of the diodes takes into account the energy loss due to the reflection of the beam on the entrance window of the chamber. Other parasitic reflections on the prism surfaces are easily calculated, and the true value of the energy hitting the rear face of the film during SPW excitation experiments may be accurately known.

The spectral sensitivity σ of the free Al surface, expressed in ampere watt^{-1} is derived from the photocurrent I_e and the incident power flux ϕ_i by the relation $\sigma = I_e/\phi_i$. ϕ_i is typically in the 10^{-8}-W range, and I_e varies in the domain 10^{-10}–10^{-13} A. From σ and the photon energy $\hbar\omega$, the quantum yield Q (expressed in electrons per incident photon) is easily obtained:

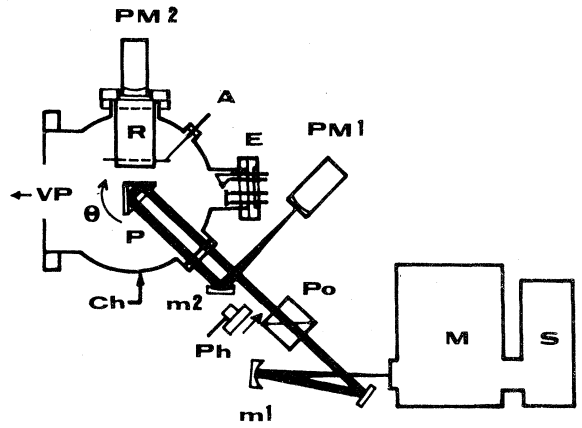

FIG. 3. Experimental setup. *Ch*, UHV chamber; *VP*, vacuum pumps; *E*, Al and Cs evaporators; *R*, scattered photons collector; PM_1 and PM_2, photomultipliers; *P*, silica prism; *A*, electron collecting anode; *S*, light source; *M*, grating monochromator; m_1 and m_2, cylindrical mirrors; P_0, polarizer; *Ph*, Si (or Ge) photodiode.

$$Q = \sigma \frac{\hbar\omega}{e},$$

where e is the electronic charge.

After baking the whole vacuum setup for 24 h at 300 °C, the Al and Cs evaporators are separately outgassed during 15 min, at temperatures slightly below the respective evaporation temperatures of these metals with an opaque shield inserted between the hot sources and the prism. Al is then evaporated from pieces of 99.99%-pure Al wire, at a rate of about $2\,\mathrm{nm\,s^{-1}}$, to a final thickness of $d = 17 \pm 1$ nm. During deposition, the pressure rises to 5×10^{-9} Torr and after the end of the evaporation process decreases in a few minutes to its nominal value ($p < 5\times10^{-11}$ Torr).

In order to compute Al optical constants and accurate values of the film thickness d, SPW are excited at the metal–vacuum interface by the ATR method, and the reflectance curves $R_p(\theta)$ are recorded at various wavelengths from $\lambda = 300$–1200 nm. At room temperature, Al films show no perceptible annealing effects, as evidenced by the excellent reproducibility of $R_p(\theta)$ curves obtained after evaporation, and delays of 24 h or even more, respectively.

To lower the work function of the Al surface, a tiny quantity of Cs is then slowly evaporated, corresponding to an equivalent mass thickness of a fraction of an nm in about 20 min. During the deposition of Cs atoms on the Al surface, the photoemission current I_e is continuously recorded, and evaporation is stopped when I_e attains its maximum, following a technique generally used by photocathode manufacturers and many authors for the Cs activation of metal (tungsten,[38] nickel,[39] or silver[40]) or semiconductor surfaces.[41,42] As far as we know, nothing has been published to date on Cs activation of Al films in UHV.

During the Cs evaporation, the photoelectric threshold wavelength λ_s increases from about 300 to 820 nm. The corresponding value of the final work function ($W_\phi = 1.5$ eV) is smaller than that for a thick Cs layer[43] ($W_\phi = 2.1$ eV). For about 24 h, following the Cs deposition, a very slow evolution of λ_s up to 825 nm is observed. At the same time the photoyield slightly increases. Then very stable electrical properties of the surface are obtained, both the electron emission and the threshold wavelength remaining stable for weeks, provided that the residual pressure remains in the range of a few 10^{-11} Torr. However, for pressures above 10^{-10} Torr, after its initial growth the emission falls more or less rapidly, probably due to contamination of the surface.

The modification of SPW resonance curves induced by this optimum Cs overlayer is studied by recording the new reflectance curves $R'_p(\theta)$. Within a margin of error, the ultimate slow evolution of the work function W_ϕ is not accompanied by a visible variation in shape or angular position of the $R_p(\theta)$ curves, thus proving that photoelectric emission is a phenomenon more sensitive to surface perturbations than are SPW induced variations of the surface reflectivity and also the optical constants of the film.

From data given in various publications,[40,44] the superficial density of Cs atoms corresponding to a minimum value of the work function may be estimated at a few 10^{14} atoms $\mathrm{cm^{-2}}$, a value which turns out to represent a fraction of a monolayer, the equivalent mass thickness being about 0.1 nm. The vapor pressure of Cs at $T = 300$ K attains 10^{-6} Torr, and the unhampered evaporation of Cs atoms being of the order of a few 10^{14} atoms $\mathrm{cm^{-2}\,s^{-1}}$, a monatomic Cs layer would be evaporated in a time of about one second. The Cs ionization energy is inferior to the Al work function and we may reasonably assume that a layer of ionized Cs atoms is formed, the electric dipoles being responsible for the initial lowering of the work function to a value of about 1.5 eV. The further lowering of W_ϕ during the day following the Cs deposition may be explained by a dynamical equilibrium between oxygen atoms adsorbed on the cesiated surface and free oxygen molecules existing in the residual gas. Other experiments,[45] not reported here, have shown the possibility of further lowering W_ϕ to about 1 eV by increasing the partial oxygen pressure to about 10^{-9} Torr for a few minutes, thus forming a Cs-oxide layer on the surface.

The long-time stability of the activated Al surface allows accurate measurements of the photoemission properties under various illumination conditions. Indeed the complete characterization of the photoelectric parameters we need for the calculation of the photoemission currents enhanced by SPW excitation necessitates a long series of measurements as follows.

(i) Each film is first illuminated on its front face (metal–vacuum interface), and the spectral sensitivities $\sigma_p^+(\varphi)$ and $\sigma_s^+(\varphi)$ are measured with p- and s-polarized light, respectively, for three angles of incidence ($\varphi = 0°$, 45°, and 70°).

(ii) The ratio of spectral sensitivities σ_s^+ (front illumination) to σ_s^- (rear illumination) is measured at the same angle of incidence ($\varphi^+ = \varphi^- = 45°$) as a function of wavelength λ, and the electron escape length L can be computed for each value of λ.

(iii) The film being illuminated through the prism (rear illumination), the photocurrent is recorded versus θ in the ATR configuration, at a

discrete number of photon energies, with s- and p-polarized light, respectively. Only with p-polarized light are SPW excited, and a large enhancement of the photoemission current is observed. The measured total emission yield $\sigma_p^-(\varphi)$ vs φ, the incidence angle on the layer, is then compared to the corresponding theoretical values obtained from the local optical constants, with the help of phenomenological models for the volume and surface photoeffects.

IV. EXPERIMENTAL RESULTS

Typical variations of the reflectivity $R_p(\theta)$ [or $R'_p(\theta)$] for a 17-nm-thick Al film illuminated through the prism with p-polarized light are shown in Fig. 4, for the clean Al layer (solid lines) and after deposition of the Cs overlayer (dashed lines), respectively. When φ is increased beyond $\varphi \simeq 42°$, a maximum is observed, corresponding to the onset of the internal reflection at $\varphi = \varphi_L$ (experimental values of R_p and R'_p are normalized to this maximum), and then appears a deep absorption peak due to SPW excitation.

Except for a narrow wavelength domain in the vicinity of $\lambda = 800$ nm, the value of the minimum R_m remains less than 10%. The angular position of the absorption dip moves to larger angles when the wavelength λ varies from the ir to the uv domain. At the same time the half-width of the curves increases slowly, thus proving an enhanced SPW damping at higher photon energies. The anomalous results observed near $\lambda = 800$ nm are thoroughly reproducible from film to film. R_m may rise above 40% (Fig. 4) and the damping also increases, as evidenced by the widening of the dip. This anomaly corresponds to a well known local maximum of ϵ_2'', the imaginary part of the Al dielectric permittivity.

During these experiments, it was impossible to detect any scattered light either from the initial Al layer, or after Cs deposition, the scattered flux remaining less than 10^{-5} in relative value. We may conclude that our Al surfaces are smooth enough to be considered as perfectly plane.

Figure 5 shows the photoemission current $I_p(\varphi)$ variation versus φ, obtained with the cesiated film 17-nm thick, for three values of wavelength (300, 500, and 765 nm). The corresponding values of $R'_p(\varphi)$ are also shown. With increasing φ, the photocurrent slowly rises until the critical angle φ_L is reached, after which it increases

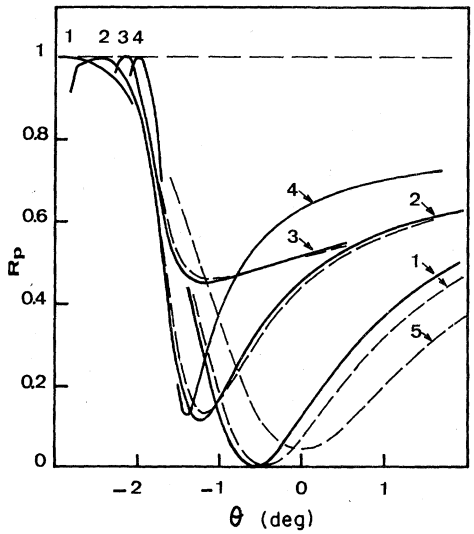

FIG. 4. Variations of the film reflectivity in p-polarized light (rear illumination) versus the angle of incidence θ of the radiation on the entrance face of the prism for various wavelengths. Continuous lines: R_p (clean Al). Dashed lines: R'_p (Cs-activated Al film). R_p (R'_p) curves are normalized to their maximum value. $\lambda_1 = 350$, $\lambda_2 = 500$, $\lambda_3 = 765$, $\lambda_4 = 1050$, $\lambda_5 = 300$ nm.

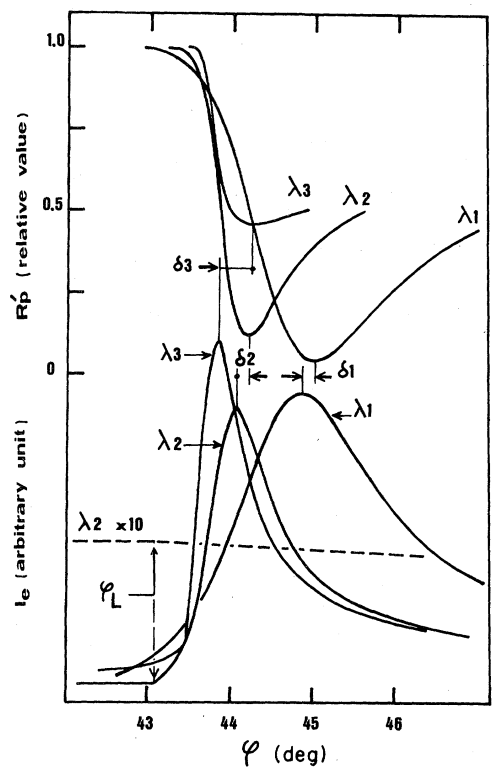

FIG. 5. Photoelectric current variations versus φ (the true incidence angle on the film surface) for three wavelengths ($\lambda_1 = 350$, $\lambda_2 = 500$, $\lambda_3 = 765$ nm) of the p-polarized incident radiation and corresponding reflectivities. $\delta 1$, $\delta 2$, and $\delta 3$ indicate the angular difference between angular position of the photocurrent peak and the minimum of the reflectivity dip. The dotted curve represents the photocurrent in s-polarized light at $\lambda_2 = 500$ nm.

dramatically, and a resonant peak is obtained. The angular position of the photocurrent peak φ_M differs slightly from φ_m, the angle for which $R'_p(\varphi)$ experienced its minimum value. The interval $\delta\varphi = \varphi_M - \varphi_m$ depends on λ and varies from 0.15° to 0.4°, the photon energy being increased. With Al films evaporated in classical vacuum and then studied in air, a similar angular shift $\delta\varphi$ has been observed in previous experiments[34] between φ_m and the scattered light peak position, in good agreement with the theoretical values obtained by computation of $R_p(\varphi)$ and the real part K'_{px} of the SPW wave vector, respectively. $\delta\varphi$ is a function of ϵ''_2 and would be zero for $\epsilon''_2 = 0$. For this reason, $\delta\varphi$ cannot be observed experimentally with Ag layers whose ϵ''_2 values are much smaller than those of Al layers. With Ag films one should obtain $\delta\varphi \simeq 0.02°$, an angular shift barely accessible to experimentation.

As the angular shift $\delta\varphi$ is always present for high absorption metals (such as Al, Au, and In), the method generally used to determine SPW dispersion curves from the φ_m values of the $R_p(\varphi)$ curves leads to incorrect results, especially in the vicinity of ω_{sp}. Surprisingly, and despite the anomalous width of the $R_p(\varphi)$ curve corresponding to $\lambda = 756$ nm, the half-height width of the photocurrent peak continuously decreases from the uv to the ir domain.

If s-polarized light is now used, the experimental curves $I_s(\varphi)$ no longer have a maximum. An example is given in Fig. 5 for $\lambda = 500$ nm. In the angular range $\varphi \leq \varphi_L$ a plateau is observed, σ_s^- and σ_p^- having in this region similar values, and for $\varphi > \varphi_L$, I_s slowly decreases. Without excitation of SPW, the photosensitivity of the film would be given approximately by $\sigma_p^- \simeq \sigma_p^-(\varphi_L)$, and the maximum gain of sensitivity due to SPW for a cesiated film may attain $\sigma_p^-(\varphi_m)/\sigma_p^-(\varphi_L) \simeq 20$.

Changing now from rear to front illumination the spectral sensitivities $\sigma_p^+(\lambda)$ and $\sigma_s^+(\lambda)$ are measured as a function of λ for three angles of incidence ($\varphi = 0°$, 45°, and 70°). The angle of incidence being constant, σ_p^+ and σ_s^+ are measured in succession for each wavelength in the energy range $1.5 < \hbar\omega < 4$ eV. With this procedure, the geometrical characteristics of the beam remain unchanged when the polarizer is rotated and the illuminated area on the film (and on the photodiode) is rigorously the same for both polarizations. As a consequence the ratio σ_p^+/σ_s^+, which is independent of the spectral sensitivity of the photodiode, may be obtained with good accuracy—essentially limited by the noise and the linearity of the amplifiers—the uncertainty being estimated to be 1%.

Experimental results are given in Fig. 6. Spectral sensitivities $\sigma_s^+(\lambda)$ increase monotonically from threshold to the uv and decrease with angle of incidence. At a fixed wavelength σ_p^+ is always greater than σ_s^+, for a given incidence angle (except for $\varphi = 0$, both sensitivities being equal in this case). In addition, σ_p^+ increases continuously with φ, from $\varphi = 0°$ to 70°.

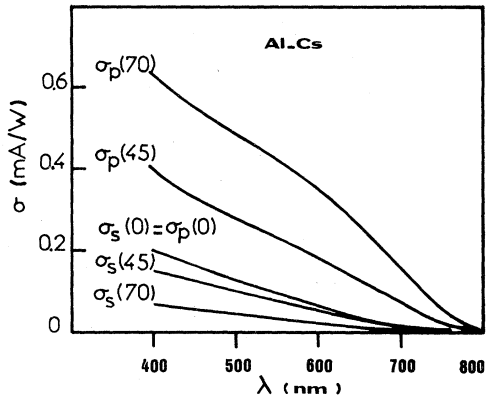

FIG. 6. Spectral sensitivity of the cesiated Al film illuminated on its front face for three values of the incidence angle φ ($\varphi = 0°$, 45°, 70°). σ_p^+: p-polarized light; σ_s^+: s-polarized light.

V. OPTICAL MODEL FOR THE Al-Cs LAYERS

In order to calculate the absorbed energy distribution in the Al film, a model is needed which takes into consideration as exactly as possible the geometrical and optical characteristics of the Al thin layer covered by a discontinuous layer of Cs atoms. An important result should be emphasized: shape variation and angular shift of the absorption dips obtained with clean Al and stabilized Al-Cs surfaces, respectively, are always very small (see, for example, Fig. 4).

Denoting by R_m, φ_m and R'_m, φ'_m the coordinates of the minimum in the $R_p(\varphi)$ and $R'_p(\varphi)$ curves, respectively, measured values of these parameters are reported in Table I, with uncertainties $\delta R \leq 4 \times 10^{-3}$ and $\delta\varphi \leq 2 \times 10^{-2}$ degree. The absence of scattered light, together with the weakness of the perturbation of the Al surface reflectance by the Cs overlayer, allows us to at-

TABLE I. Minimum reflecting power of an Al film 17-nm thick.

	Clean Al		Al-Cs	
λ (nm)	R_m	φ_m (deg)	R'_m	φ'_m (deg)
350	0.000	44.62	0.002	44.70
500	0.115	44.15	0.130	44.21
750	0.449	44.20	0.460	44.24

tempt to calculate the permittivity ϵ_2 and the thickness d of the Al-Cs film by using the very simple model shown in Fig. 2, consisting of a homogeneous thin film with perfectly smooth plane parallel surfaces, thus neglecting the presence of Cs atoms.

In order to compare the theoretical variations of the reflectivity versus φ with the experimental curves $R_p(\varphi)$ [or $R'_p(\varphi)$], it is necessary to compute the relative reflectivity $X(\varphi)$ normalized to the maximum value $R(\alpha)$ obtained for $\varphi = \alpha \simeq \varphi_L$:

$$X(\varphi) = R(\varphi)/R(\alpha) .$$

The theoretical curve $X(\varphi)$ may approximate the experimental one $R_p(\varphi)$ for a single set of the three parameters ϵ'_2, ϵ''_2, and d within a margin of error $\delta\epsilon'_2$, $\delta\epsilon''_2$, and δd.

Starting from arbitrary values ϵ'_s, ϵ''_s (which may be the values corresponding to bulk Al), and d_s (the thickness given by the quartz thickness monitor) an iterative program adjusts in sequence the three parameters, until the quadratic deviation $\bar{e}$ between $X(\varphi)$ and $R_p(\varphi)$ attains its minimum. Choosing N equidistant points separated by $\Delta\varphi$ (with $15 < N < 20$), $\bar{e}$ is defined by

$$\bar{e}^2 = \frac{1}{N}\sum_{k=0}^{N-1} [X(\alpha + k\Delta\varphi) - R_p(\alpha + k\Delta\varphi)]^2 .$$

We postulate that the model in use for the computation is realistic if the following conditions are both fulfilled: (i) $\bar{e}$ must stay within the experimental uncertainties $2\delta R_p$ and (ii) the optical calculated film thickness $(d \pm \delta d)$ must be a constant whatever the wavelength may be.

Typical results obtained in the energy range $1.2 < \hbar\omega < 3.5$ eV and $1.6 < \hbar\omega < 4$ eV for a clean Al surface and a Cs-covered surface, respectively, are given in Table II for a few values of λ.

These results show that values of $\bar{e}$ are always in the domain $3 \times 10^{-3} < \bar{e} < 8 \times 10^{-3}$, and never very different from δR_p for the clean Al as well as for the cesiated Al layer. Taking into account the other uncertainties ($\delta\varphi \leq 0.02°$, $\delta n_1 \leq 10^{-4}$, $\delta\lambda \leq 0.5$ nm) we obtain the probable errors of the real and imaginary parts of ϵ_2, respectively: $\delta\epsilon'_2$, $\delta\epsilon''_2$, and of the thickness δd. Figure 7(a) shows a plot of d versus the incident photon energy $\hbar\omega$ for an Al film and for the same film covered with Cs atoms. Although the uncertainty δd grows from 0.5 nm in the uv domain to 1.5 nm at the other end of the spectral domain, we may consider that (i) the optical thickness d is a constant and is known with an accuracy of ± 0.5 nm (a factor 2 times better than the accuracy given by the quartz thickness monitor) and (ii) the calculated thickness remains unchanged when the Cs layer is grown on the Al surface, within the same uncertainty limit of ± 0.5 nm. This result confirms the hypothesis of a submonolayer Cs coverage.

The variations of ϵ'_2 and ϵ''_2 as functions of the photon energy are shown in Fig. 7(b) for a film of thickness $d = 17 \pm 0.5$ nm, and compared to the results published by Mathewson and Myers[46] for bulk Al. We emphasize that the relative perturbation of the "average" permittivity of the film that can be observed after the buildup of the thin Cs overlayer never exceeds 5% and remains within the limits of the calculated uncertainties $\delta\epsilon'_2$ and $\delta\epsilon''_2$.

From these results, we may conclude that the

TABLE II. Typical uncertainties on ϵ'_2, ϵ''_2, and d.

λ (nm)		$\bar{e}$ (10^{+2})	$\epsilon'_2 \pm \delta\epsilon'_2$	$\epsilon''_2 \pm \delta\epsilon''_2$	$d \pm \delta d$ (nm)
Al	350	0.7	-17.2 ± 0.3	2.94 ± 0.15	17.7 ± 0.7
Al-Cs		0.6	-16.7 ± 0.3	2.92 ± 0.15	17.4 ± 0.5
Al	600	0.8	-51.0 ± 0.5	17.7 ± 0.8	17.1 ± 0.4
Al-Cs		0.4	-49.6 ± 0.6	19.1 ± 1	17.5 ± 0.6
Al	765	0.35	-66.0 ± 3	46 ± 4	16.8 ± 0.8
Al-Cs		0.4	-64.5 ± 3	48.6 ± 5.3	16.7 ± 0.8

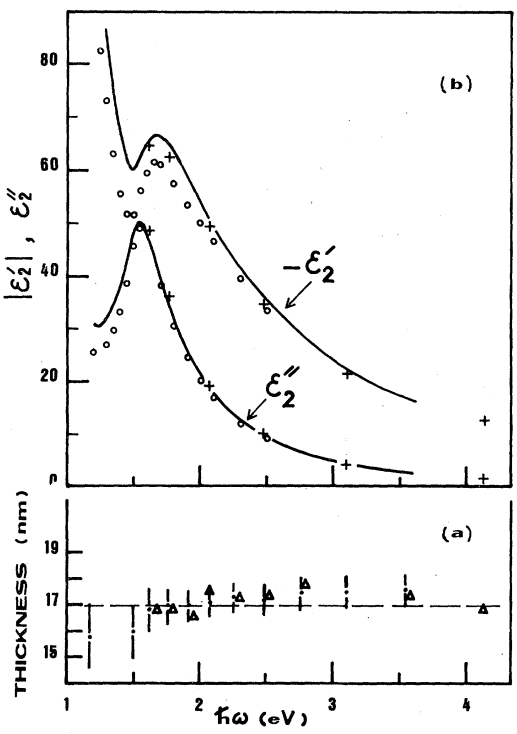

FIG. 7. Optical parameters of the Al film 17-nm thick versus $\hbar\omega$. (a) Calculated thickness d (••• clean Al film; ΔΔΔ cesiated film). (b) Real and imaginary parts of the dielectric constant (— Al; +++ Al-Cs; ooo bulk Al, Mathewson and Myers, Ref. 45).

simple one-layer system is convenient and accurate enough for the calculation of optical parameters, provided that we use the average permittivity of the Al-Cs layer. The same one-layer model will be used for computing the photoemission yield.

VI. VOLUME AND SURFACE PHOTOEFFECTS

Following Endriz and Spicer[3] we assume that in a free-electron-like metal such as Al, surface and volume photoeffects are independent phenomena. When both effects are present, the total quantum yield is simply given by

$$T = Q + S$$

in which Q and S are the quantum yields (in electrons per incident photon) of the volume and surface photoeffects, respectively.

To calculate the contribution of the volume effect, we shall use the classical three-step model described in Sec. I. The probability for an electron photoexcited at distance z from the surface to cross the potential barrier is given by the empirical law

$$p(z) = C \exp(-z/L)$$

in which the escape length L is supposed to be independent of the final energy of the excited electron at constant photon energy; C is a constant which depends only on the photon energy (not on the angle of incidence, nor on the polarization state of the incident radiation).

Denoting by $\eta(z, \varphi)$ the density of photons absorbed in the film at distance z below the surface, normalized to unit photon flux, we may write

$$Q(\varphi) = C \int_0^d \eta(z, \varphi) \exp(-z/L) dz ,$$

where d is the film thickness. $\eta(z, \varphi)$ may be easily calculated from the classical Maxwell's equations with local boundary conditions.

If E_i^+ and E_i^- are the complex amplitudes of the electric field vectors of the waves moving in medium i from and towards the surface ($z = 0$), respectively, the total electric field vector $E_2(z)$ inside the metal is given by

$$E_2(z) = E_2^+(z) + E_2^-(z) ,$$

provided account is taken for the multiple reflections at the two interfaces. Finally

$$\eta(z, \varphi) = \frac{2\pi \epsilon_2''}{\lambda \cos\varphi} \left| \frac{E_2(z, \varphi)}{E_1^+} \right|^2 .$$

λ is the vacuum wavelength and E_1^+ the electric field amplitude of the incident radiation.

s-polarized light has a single-field component E_y parallel to the surface. p-polarized light has a parallel component E_x and a component E_z normal to the surface (see Fig. 2).

Associating to each field component a part of the absorbed energy we write

$$\eta_s(z) = \eta_y(z) ,$$

$$\eta_p(z) = \eta_x(z) + \eta_z(z) .$$

Complete expressions for $\eta(z)$ may be found in Refs. 9 and 47.

The quantum efficiency corresponding to front illumination of the film is then obtained, and may be written

$$Q^+(\varphi) = C F^+(\varphi, L) .$$

$F^+(\varphi, L)$ may take two different forms, $F_s^+(\varphi, L)$ or $F_p^+(\varphi, L)$, according to the polarization state of the incident light.

For illumination through the prism, the above calculations are still valid, provided that in the evaluation of $\eta(z, \varphi)$ ϵ_1 and ϵ_3 are exchanged and the distance z is replaced by the complementary distance $(d - z)$. The new quantum yield is, therefore,

$$Q^-(\varphi) = C \int_0^d \eta(z, \varphi) \exp\left(-\frac{d - z}{L}\right) dz ,$$

$$Q^-(\varphi) = C \exp\left(-\frac{d}{L}\right) F^-(\varphi, L) .$$

For a given energy $\hbar\omega$, the escape length being known, the corresponding values of $F(\varphi, L)$ are calculated from the local optical constants of the Al films.[48] They are sufficient to represent the angular variations of the volume photoyield for each light polarization state.

In order to compare to the experimental results concerning spectral sensitivities σ, we shall recall that Q and σ are bound simply by the relation

$$Q = \sigma \frac{\hbar\omega}{e} .$$

The surface photoeffect originates from the direct excitation of free electrons by the E_z field component at the metal-vacuum interface, and the associated photoyield is given by[3,12]

$$S(\omega, \varphi) = K(\omega) \eta_z(0, \varphi) .$$

$K(\omega)$ is a characteristic coefficient that depends only on the photon energy and is assumed to be independent of the incidence angle φ. $\eta_z(0, \varphi)$ is the part of the absorbed energy density in the metal, associated with the E_z component only and calculated in $z = 0$ (front illumination). This function, which depends upon the optical constants of the metal and the incidence angle φ, is proportional to the squared amplitude of the E_z field at $z = 0$: $\eta_z(0, \varphi) \sim |E_z(0, \varphi)|^2$ and may be easily calculated

for an incident unit photon flux.

For forward illumination of the film we have

$$S_p^+(\varphi) = K(\omega)\eta_z^+(0,\varphi),$$

while for rear illumination

$$S_p^-(\varphi) = K(\omega)\eta_z^-(d,\varphi).$$

(We shall assume that the surface effect exists only with p-polarized illumination.)

In order to perform quantitative calculations, the parameters C, L (volume effect), and $K(\omega)$ (surface effect) have to be determined as a function of incident photon energy $\hbar\omega$. This is possible only if both effects may be fully differentiated with the help of their polarization dependence.

Consequently the following procedure is used.

(i) After careful control that photoelectric measurements in s polarization are free of any surface effect, the measured photoemission current is assumed to be a pure volume-effect contribution. The length L is then computed from photoelectric measurements carried out with s-polarized light in front and rear illumination. The parameter C is known from the measured value of the photoemission current together with the calculated value of the function $F_s^+(\varphi)$.

(ii) The volume photoeffect contribution $F_p^+(\varphi)$ in p-polarized light illumination is computed together with its spectral sensitivity variations in front illumination for $\varphi^+ = 45°$ and 70°, respectively, the parameters C and L being assumed independent of the light polarization.

(iii) Finally, the surface contribution may be obtained by subtraction of the volume effect contribution from the experimental values of the total spectral sensitivities σ_p^+ (see Fig. 6). The surface photoexcitation parameter $K(\omega)$ is then computed.

An excellent proof of the total absence of a surface-effect contribution to the photoemission due to s-polarized light illumination is found in the comparison between experimental and theoretical variations of the quantum photoyield versus the incidence angle φ. For a pure volume effect, the angular variations of Q_s^+ may be characterized for each value of λ by the ratio $Q_s^+(\varphi)/Q_s^+(0) = F_s^+(\varphi, L)/F_s^+(0, L)$. This ratio, which is independent of C, contains L as an unknown parameter. However, numerical computation performed for various values of L chosen in a wide domain, $1 < L < 19$ nm, shows that the result is nearly independent of L. A few examples are given in Table III for various wavelengths.

In our experiments, photon energies are far below $\hbar\omega_p$ and the high values of ϵ_2 make the wave vector of the refracted light in the metal nearly normal to the surface whatever φ may be. The escape length L being a constant at fixed wavelength, the ratio $Q_s^+(\varphi)/Q_s^+(0)$ becomes nearly independent of L. This would not be necessarily true at higher photon energies.

TABLE III. Calculated values of the photoyield in s-polarized light for two values of the escape length L.

	$Q_s^+(70)/Q_s^+(0)$		$Q_s^+(45)/Q_s^+(0)$	
λ (nm)	$L = 1$ nm	$L = 19$ nm	$L = 1$ nm	$L = 19$ nm
350	0.3790	0.3772	0.7438	0.7418
500	0.3716	0.3713	0.7358	0.7354
750	0.3759	0.3772	0.7392	0.7404

Table III confirms that the volume-effect contribution decreases readily when φ is increased from 45° to 70°. In contrast, the photocurrent that could arise from a surface effect would grow as a function of φ like $\eta_z(0,\varphi)$. If some roughness-aided surface effect were present, one would observe a strong deviation between experimental and calculated values of the photoyield reported in Table III.

Figure 8 shows the variations of the measured spectral sensitivities (dots) $\sigma_s^+(\varphi)/\sigma_s^+(0)$ as a function of λ and the values of the photoyields $Q_s^+(\varphi)/Q_s^+(0)$ (solid lines) calculated with the hypothesis of a pure volume effect. The area of the illuminated region on the sample increases by a factor of 3 when φ varies from 0° to 70°, and local variations of the spectral sensitivity may induce systematic errors in the measurements. As the experimental and theoretical results are in good agreement within a maximum deviation less than 15%, we may reasonably conclude that in our films the photoemission current obtained with s-polarized light has its origin in a pure volume effect.

In order to determine the electron escape length L we have now to compare the quantum yields with s-polarized light corresponding to front and rear illumination. The incidence angle being kept constant ($\varphi_1^+ = \varphi_1^-$) in both cases, this procedure leads to a minimum uncertainty on the experimental ratio

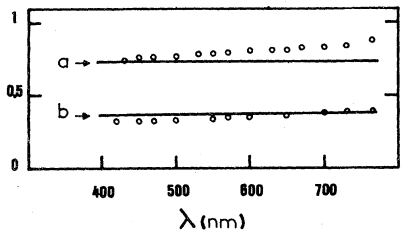

FIG. 8. Variations of the volume photoeffect contribution versus the light wavelength λ [— calculated values $Q_s^+(\varphi)/Q_s^+(0)$; ○ ○ ○ experimental values $\sigma_s^+(\varphi)/\sigma_s^+(0)$ from Fig. 6]. (a) $\varphi = 70°$, (b) $\varphi = 45°$.

$$\beta(\varphi_1) = \sigma_s^+(\varphi_1)/\sigma_s^-(\varphi_1) .$$

In the corresponding theoretical ratio the only unknown parameter is the escape length L:

$$\alpha(\varphi_1) = \frac{Q_s^+(\varphi_1)}{Q_s^-(\varphi_1)} = \exp\left(\frac{d}{L}\right)\frac{F_s^+(\varphi_1, L)}{F_s^-(\varphi_1, L)} .$$

Taking $\varphi_1 = 45°$, the variations of $\alpha(45)$ as a function of L are reported in Fig. 9 for three values of the photon energy $\hbar\omega$. By identifying $\beta(45) \equiv \alpha(45)$, the escape length $L(\hbar\omega)$ may be obtained from curves similar to those of Fig. 9, and the results are given in Fig. 10. The uncertainty of $\beta(45)$ never exceeds $\pm 1\%$. Taking into account the respective uncertainties affecting the optical constants ($\delta\epsilon_2'$, $\delta\epsilon_2''$) and the thickness (δd), calculated accuracy limits are also reported in Fig. 10.

To our knowledge, in the energy domain covered by our experiments no other experimental results concerning L in Al have been published to date. For higher energies ($4.5 < \hbar\omega < 10$ eV) L was measured by Calcott and Arakawa.[49] Their results have also been plotted in Fig. 10 and appear in excellent agreement with ours: Both series of results are located on the same curve.

The most striking result is the rapid variation of L in this energy domain: L falls from 13 to 2 nm, while $\hbar\omega$ varies from 1.5 to 10 eV. Since the mean-free-path values for electron-phonon collisions in Al (Ref. 24) are much greater than the L values, we may assume safely that L is essentially determined by electron-electron collisions.

Coming now to the surface effect in p-polarized illumination on the front face of the Al film, its contribution may be easily calculated from the

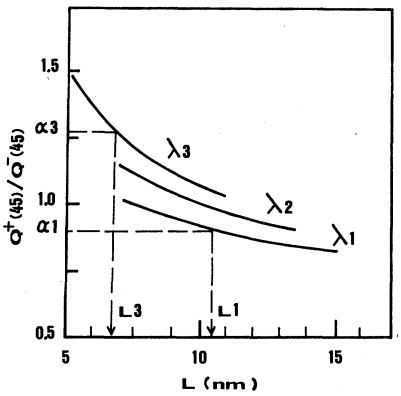

FIG. 9. Ratio of photoemission yields for front and rear illumination with s-polarized light as a function of the electron escape depth L for the incidence angle $\varphi = 45°$ and various wavelengths λ ($\lambda_1 = 750$, $\lambda_2 = 500$, $\lambda_3 = 350$ nm).

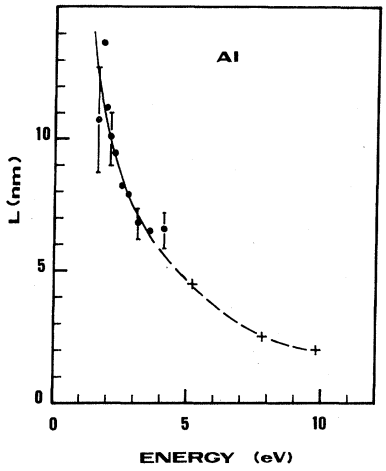

FIG. 10. Electron escape depth in Al (○○○ our results; +++ Calcott and Arakawa, Ref. 48) as a function of the mean energy of the photoexcited electron above the Fermi level.

measured values of $\sigma_p^+(\varphi)$ and $\sigma_s^+(\varphi)$. Denoting now by Y the theoretical volume photoeffect sensitivity (in A/W), and assuming that in s-polarized light, photoemission is a pure volume effect, we may write

$$Y_s^+(\varphi) \equiv \sigma_s^+(\varphi) .$$

The theoretical contribution of the volume effect in p-polarized light may be calculated for each value of φ ($\varphi = 45°$ and 70°), assuming that C and L do not depend on the polarization state of the incident radiation

$$Y_p^+(\varphi) = \sigma_s^+(\varphi)\frac{F_p^+(\varphi, L)}{F_s^+(\varphi, L)} .$$

Values of L are taken from Fig. 10. As the ratio

$$r(\varphi) = \frac{F_p^+(\varphi, L)}{F_s^+(\varphi, L)}$$

is nearly independent of L in the whole domain of wavelengths, the uncertainty in $r(\varphi)$, essentially due to the errors in the optical constants of the film, never exceeds 0.5%. On the other hand, the ratio of experimental spectral sensitivities

$$s(\varphi) = \frac{\sigma_p^+(\varphi)}{\sigma_s^+(\varphi)} ,$$

which is independent of the calibration of the photodiode, is measured at a constant angle of incidence φ with an accuracy of about $\pm 1\%$.

By comparing $r^+(\varphi)$ to $s^+(\varphi)$, a large contribution of the surface photoeffect is evidenced. For example, at $\lambda = 500$ nm the following values are obtained at $\varphi = 45°$ and 70°, respectively:

$$\frac{\sigma_p^+(45)}{\sigma_s^+(45)} = 2.74 \pm 0.03, \quad \frac{Y_p^+(45)}{Y_s^+(45)} = 1.80 \pm 0.01,$$

$$\frac{\sigma_p^+(70)}{\sigma_s^+(70)} = 11.2 \pm 0.1, \quad \frac{Y_p^+(70)}{Y_s^+(70)} = 5.7 \pm 0.03.$$

Figure 11 shows a plot of $\sigma_p^+(70)$ and $\sigma_p^+(45)$ vs λ, compared to $Y_p^+(70)$ and $Y_p^+(45)$, respectively. The error in $Y_p^+(\varphi)$ may be estimated to less than $\pm 1.5\%$ provided that the uncertainty on the absolute calibration of the photodiode is neglected.

The volume-effect contribution to the photosensitivity slowly increases with φ, and also with the photon energy, while it remains always lower than experimental sensitivity $\sigma_p^+(\varphi)$. The relative deviation

$$v^+(\varphi) = \frac{\sigma_p^+(\varphi) - Y_p^+(\varphi)}{Y_p^+(\varphi)}$$

reaches its maximum near the threshold and decreases monotonically with λ.

The spectral sensitivity of the surface photoeffect $S_p^+(\lambda)$ is obtained by writing

$$S_p^+(\lambda) = \sigma_p^+(\lambda) - Y_p^+(\lambda)$$

Graphs of the behavior of $S_p^+(\lambda)$ will be found in Fig. 12 for $\varphi = 45°$ and 70°. They show unambiguously that the surface-effect contribution sharply increases with the angle of incidence $[S_p^+(70)/S_p^+(45) \simeq 3]$ and represents the major part of the global photoemission when the incident photon energy decreases to values close to the threshold. In contrast, in the uv domain, the ratio $S_p^+(\varphi)/Y_p^+(\varphi)$ drops to values lower than unity.

The coefficient $K(\omega)$ is then computed, using the values of S_p^+ and $\eta_s(0, \varphi)$, and the results are shown in Fig. 13 for $\varphi = 45°$ and 70°. At first sight, for a given photon energy, $K(\omega)$ may take two values

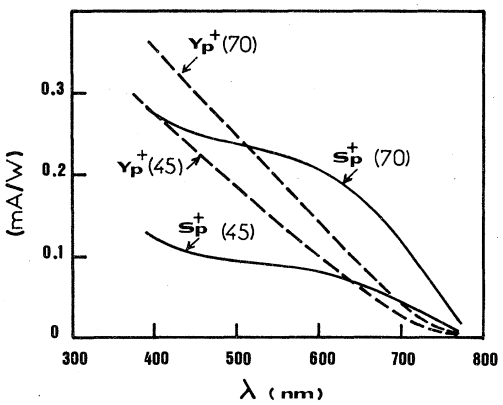

FIG. 12. Volume and surface photoeffects for an Al-Cs surface in p-polarized light (front illumination) and two distinct angles of incidence $\varphi = 45°$ and 70°.

depending upon the angle of incidence φ, in apparent contradiction with our initial hypothesis. However, we observe that the curves $K_{45}(\omega)$ and $K_{70}(\omega)$ are similar with a common location of their maximum value at $\hbar\omega = 2.1$ eV. Moreover the deviation between them never attains 15% in relative value. Emphasizing again the difficulty in comparing results corresponding to very different incidence angles we may consider that the observed variation of $K(\omega)$ vs φ remains within our uncertainty limits, and that $K(\omega)$ does not depend upon φ, in agreement with other results by Vernier *et al.*[50] concerning photoemission from Ag films. The validity of this assumption will be demonstrated *a posteriori* by the results obtained with rear illumination and SPW excitation in a narrower domain of angular variations.

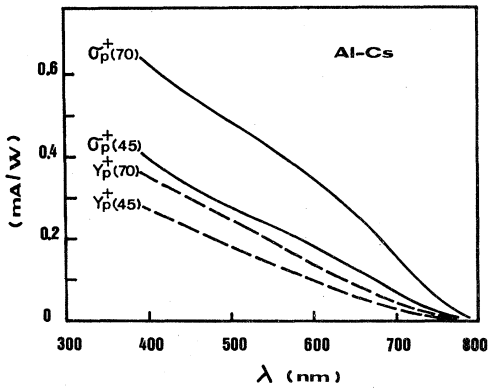

FIG. 11. Spectral sensitivity of a cesiated Al surface in p-polarized light (front illumination at $\varphi = 45°$ and 70°). $Y_p^+(\varphi)$ is the calculated volume effect; $\sigma_p^+(\varphi)$ the measured value of the total sensitivity.

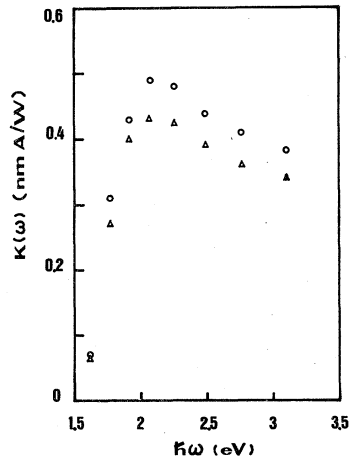

FIG. 13. Surface-effect photoexcitation coefficient $K(\omega)$. ○ ○ ○ $\varphi = 45°$; △ △ △ $\varphi = 70°$.

VII. QUANTITATIVE INTERPRETATION OF THE SPW ENHANCED PHOTOEFFECT

We first consider the volume-effect contribution to the photocurrent. A study of absorbed energy distributions $\eta_s^-(z)$ and $\eta_p^-(z)$ inside the metal film illuminated through the prism helps in understanding the volume effect behavior in the presence of SPW. Figure 14 shows a plot of the computed distribution curves at $\lambda = 500$ nm for several values of φ.

In s-polarized light $\eta_s^-(z)$ exponentially decreases inside the film (dashed curve). The reflectivity R_s being close to unity, the magnitude of the absorbed energy density remains weak, with its maximum at the metal–prism interface. In the small angular domain considered in Fig. 14, $\eta_s^-(z)$ is nearly independent of φ.

Far from the SPW resonance angle, the curves $\eta_p^-(z)$ also decrease from the prism to the metal–vacuum interface. For example, at $\varphi_L = 43.13°$, $\eta_p^-(z)$ falls continuously to a negligible value at $z = d$. This situation is profoundly modified when φ approaches the SPW excitation domain, as $\eta_p^-(z)$ has its maximum near the free surface of the film. The absolute maximum of $\eta_p^-(d)$ is obtained for $\varphi_2 = 44.10°$. Increasing φ beyond φ_2, $\eta_p^-(d)$ decreases while $\eta_p^-(0)$ slowly increases.

In order to compute the contribution of the volume effect $Y_p^-(\varphi)$ in p-polarized light, we assume again that in s-polarized illumination the volume effect is wholly responsible for the total photoemission and by writing (at $\varphi = 45°$):

$$\sigma_s^-(45) \equiv Y_s^-(45) = C \exp\left(-\frac{d}{L}\right) F_s^-(45, L) .$$

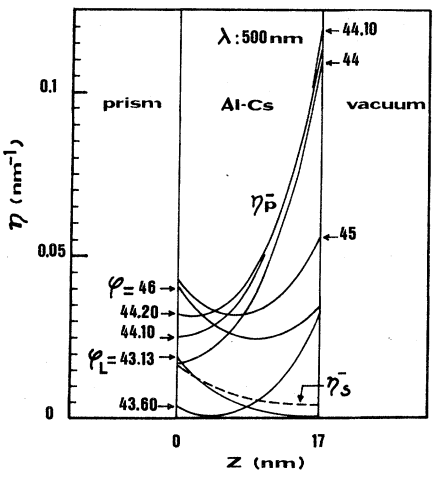

FIG. 14. Absorbed density repartition $\eta_p^-(z)$ in a thin Al film illuminated through the prism at various angles of incidence φ for $\lambda = 500$ nm. Full lines: p-polarized light. Dotted line: s-polarized light [no appreciable variation of $\eta_s^-(z)$ in the angular domain $\varphi_L < \varphi < 46°$].

$Y_p^-(\varphi)$ is given by

$$Y_p^-(\varphi) = \sigma_s^-(45)\, \frac{F_p^-(\varphi, L)}{F_s^-(45, L)} .$$

In contrast to the monotonic variation of $\sigma_s^-(\varphi)$ an important resonance peak of the volume effect contribution in p-polarized light appears, having its origin in the strong enhancement of energy absorbed by excitation of the SPW. An example is given Fig. 15 at $\lambda = 500$ nm, taking into account the experimental values $d = 17 \pm 0.5$ nm, $L = 8.5 \pm 1$ nm, and the experimental uncertainties in both parameters (the comparatively weaker uncertainty in ϵ_2 may be neglected). The curve representing $Y_p^-(\varphi)$ vs φ is located inside the cross-hatched area, and the maximum relative uncertainty in $Y_p^-(\varphi)$ remains less than $\pm 10\%$.

Represented in the same figure are the reflectivity $R_p'(\varphi)$ and the experimental photosensitivity $\sigma_p^-(\varphi)$. The comparison between curves representing $Y_p^-(\varphi)$ and $\sigma_p^-(\varphi)$ brings out several points which deserve comment. (i) The volume effect accounts for only 50% of the experimental peak at $\lambda = 500$ nm, this contribution dropping down to 20% for $\lambda = 765$ nm (a wavelength near the threshold). (ii) A minimum is observed in the curve $Y_p^-(\varphi)$ in the vicinity of the critical angle $\varphi_L = 43.13°$ before rising to its peak value, in disagreement with the experimental curve $\sigma_p^-(\varphi)$ which increases continuously to its maximum value. (iii) The angular positions of the experimental and calculated peaks are not coinciding, and the difference between them is well outside the uncertainty range. The peak value of $\sigma_p^-(\varphi)$ occurs for $\varphi_M = 44.05° \pm 0.02°$,

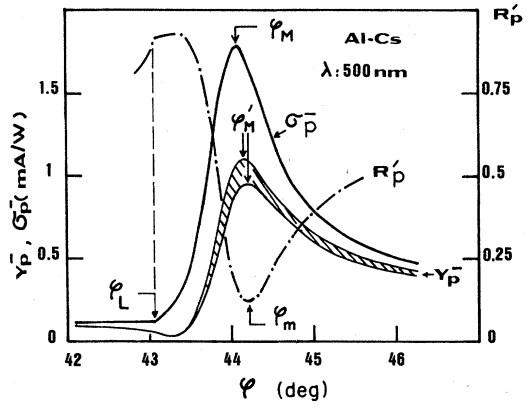

FIG. 15. SPW resonance curves at $\lambda = 500$ nm for a cesiated Al surface. σ_p^- is the measured spectral sensitivity; Y_p^- the theoretical values of the volume-effect contribution, taking into account the uncertainties on d and L calculated values. R_p' is the reflectivity (unnormalized experimental curve). The respective angular positions of the peaks are not in coincidence ($\varphi_M < \varphi_M' < \varphi_m$).

while the $Y_p^-(\varphi)$ maximum is located at φ'_M with $44.14° < \varphi'_M < 44.20°$ so that $\varphi'_M - \varphi_M \simeq 0.1°$.

Points (i) and (ii) have already been emphasized by Calcott and Arakawa[48] for Al in the uv domain of photon energies, the discrepancy between $\sigma_p^-(\varphi)$ and $Y_p^-(\varphi)$ being ascribed to a strong surface effect. To our knowledge, point (iii) was not reported before.

From Fig. 15, it is noteworthy that the incidence angle φ_m for which the reflectivity attains its minimum differs slightly from φ'_M, the angle making the volume effect maximum. The difference $\varphi_m - \varphi'_M$ may be related to the variations of the absorbed energy distributions $\eta_p^-(z)$ (see Fig. 14). Reflectivity R and total absorption A are connected by the simple relation

$$R = 1 - A = 1 - \int_0^d \eta_p^-(z)dz \, .$$

A corresponds to the area located between the curve $\eta_p^-(z)$ and the z axis and attains its maximum for $R = R_m$ at $\varphi = \varphi_m = 44.20°$, while the absolute maximum of $\eta_p^-(z = d)$, the energy density at the metal-vacuum boundary, occurs at $\varphi = \varphi_s = 44.10°$. In the simple case $L \ll d$, $Y_p^-(\varphi)$ would be proportional to $\eta_p^-(z = d)$, and would attain its peak value at $\varphi = \varphi_s$. On the contrary, with the hypothesis $L \gg d$, all excited electrons have the same probability of reaching the surface, and $Y_p^-(\varphi)$ would be closely proportional to the total energy absorbed in the film, with its maximum value at $\varphi = \varphi_m = 44.20°$.

From this discussion it follows that the resonant volume photoeffect induced by SPW excitation by itself is not able to account for either the magnitude or the shape of the experimental photocurrent $\sigma_p^-(\varphi)$. The theoretical surface-effect contribution will be proportional to $\eta_z^-(d, \varphi)$, the energy density associated with the E_z component of the electric field in the metal at the metal-vacuum boundary, assuming that $K(\omega)$ remains independent of φ. Figure 16 shows the variations of $\eta_z^-(d, \varphi)$ and $\eta_z^+(0, \varphi)$ at $\lambda = 500$ nm as a function of φ in the domain $42° < \varphi < 46°$. For front illumination of the film $\eta_z^+(0, \varphi)$ increases continuously with φ, while for rear illumination $\eta_z^-(d, \varphi)$ exhibits a strong resonant character.

As the SPW fields have their maximum located at a φ value near $\varphi^- = 45°$, we have used the values of $K(\omega)$ obtained from the preliminary experiments with $\varphi^+ = 45°$ (see Fig. 13):

$$S^-(\varphi) = K_{45}(\omega)\eta_z^-(d, \varphi) \, .$$

For $\lambda = 500$ nm, the surface-effect resonance occurs at $\varphi_2 = 43.98° \pm 0.02°$, the enhancement of the surface effect [i.e., the ratio $S^-(\varphi_2)/S^+(\varphi_2)$] being a factor of about 15.

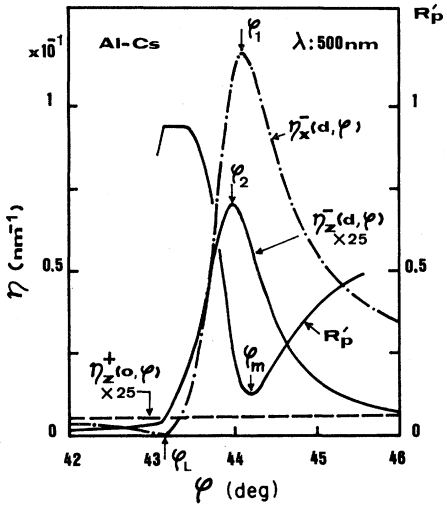

FIG. 16. Absorbed energy densities $\eta_x(d, \varphi)$ and $\eta_z(d, \varphi)$ at the metal–vacuum interface of the Al-Cs film for $\lambda = 500$ nm, related to the parallel (E_x) and normal (E_z) components of the electric field, respectively. Location of the peaks, φ_1 and φ_2 differs from the position of the R'_p minimum φ_m.

We have also represented in Fig. 16 the variations of $\eta_x^-(d, \varphi)$, the absorbed energy associated with the E_x component parallel to the metal surface at the metal-vacuum boundary, and we emphasize that the variations with φ of both components are somewhat different: (i) $\eta_x^-(d, \varphi) \sim |E_x(d, \varphi)|^2$ may exceed $\eta_z^-(d, \varphi) \sim |E_z(d, \varphi)|^2$ by a factor as high as 50, except in the vicinity of φ_L where E_x decreases to a negligible value, and (ii) the respective positions of both peaks are displaced by about 0.12°.

The E_x component of the electric field being much greater than the E_z component at the metal-vacuum boundary explains that an important additional surface effect could be induced by any roughness present on the metal surface, and in that case the preceding calculation would be inaccurate.

Figures 17(a), 17(b), and 17(c) show typical results obtained for three wavelengths, $\lambda = 765$, 500, and 350 nm, respectively. Each of these figures gives (i) the volume-effect contribution $Y_p^-(\varphi)$, (ii) the surface-effect contribution $S_p^-(\varphi)$, (iii) the total theoretical spectral sensitivity $T_p^-(\varphi)$ with

$$T_p^-(\varphi) = Y_p^-(\varphi) + S_p^-(\varphi) \, ,$$

and (iv) points related to the variations of the experimental spectral sensitivity $\sigma_p^-(\varphi)$.

From these data, and from results concerning other values of λ not reported here, several fundamental characteristics of the volume and surface effects in the presence of a surface plasma wave

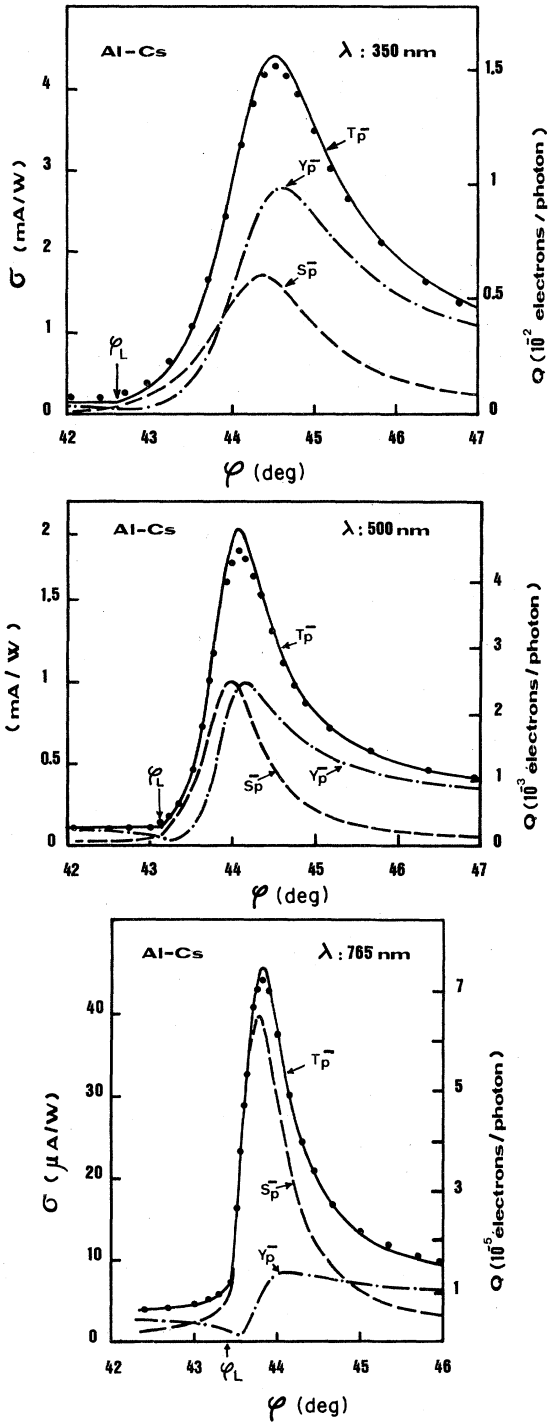

FIG. 17. Three examples of the volume- and surface-effect contributions to the total photoemission. Left ordinate scale: spectral sensitivities (S_p^- surface effect, Y_p^- volume effect, T_p^- total sensitivity, ... measured values of δ_p^-). Right scale: photoyield Q in electron per incident photon. Note the important variations in the absolute values of the photocurrents as a function of photon energy. (a) $\lambda = 350$ nm. (b) $\lambda = 500$ nm. (c) $\lambda = 765$ nm. The threshold corresponds to $\lambda \simeq 825$ nm.

can be inferred.

(i) Anywhere in the spectral range the resonance peaks in the $S_p^-(\varphi)$ curves are quite narrow and symmetrical. In contrast, the enhanced volume effect extends through a wider angular scale, and the resonance curves are asymmetrical with a long tail for $\varphi > \varphi'_M$.

(ii) Volume and surface photoeffects peaks are obtained at two distinct angles of incidence both differing from φ_M, but the total spectral sensitivity obtained by summing up both effects has its peak value located at $\varphi = \varphi_M \pm 0.02°$.

(iii) Although the separate contributions of surface and volume effects change dramatically with photon energy, the deviation existing between theoretical and experimental maximum values of the spectral sensitivity is always less than 10%.

(iv) The surface contribution increases sharply for photon energies approaching the energy threshold and may exceed the part due to the volume effect by a large factor. Figure 18 shows the variation as a function of λ of the ratio S_p/Y_p for $\varphi^+ = 45°$ and $\varphi^- \simeq 45°$ (S_p^- and Y_p^- are then the maximum values corresponding to the SPW excitation). The relative enhancement of the surface effect compared to the volume effect induced by excitation of SPW may be explained by the increased value of the ratio $E_z(0,\varphi)/E_x(0,\varphi)$ at the metal surface.

(v) At fixed wavelength, the relative value of the surface effect compared to the volume effect dramatically varies as a function of the angle of incidence φ in the angular domain of SPW excita-

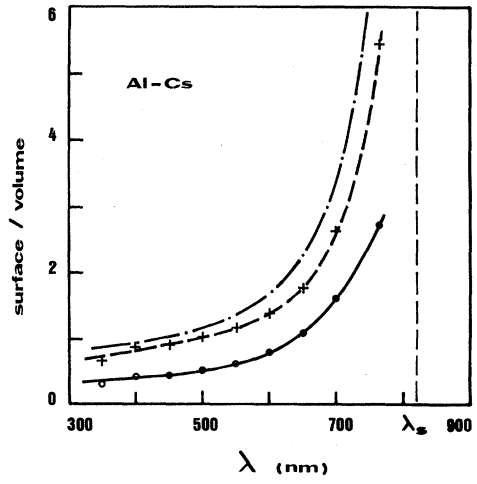

FIG. 18. Relative importance of the surface photoeffect compared to the volume photoeffect in two different situations: front illumination — experimental curve ($\varphi = 45°$), -·-·- theoretical limit value ($\varphi = 90°$); rear illumination +++ maximum excitation of the SPW ($\varphi \simeq 44°$).

tion. With increasing φ, a minimum of Y_p^- is observed at an angle just beyond the limit angle φ_L, and the ratio S_p^-/Y_p^- may attain values higher than 20 for wavelengths near threshold. At higher incidence angles ($\varphi > \varphi_M$), the relative contribution of the volume effect becomes more and more important (Fig. 19).

IX. CONCLUSION

Respective contributions of volume and surface photoeffects to the total photoemission from Al-cesiated thin films have been obtained for a surface directly illuminated by a p-polarized radiation. From these measurements, we have succeeded in calculating with good accuracy the absolute values of both effects for the same surface in which SPW are excited by using the ATR method.

The excellent agreement between computed and measured sensitivities and/or photoyields indirectly confirms the validity of our initial assumptions and of the simple models used throughout the calculation of the photocurrent as follows:

(i) The three-medium model with parallel, ideally smooth interfaces corresponding to an Al film inserted between two semi-infinite lossless dielectrics and neglecting the presence of the Cs submonolayer on the Al surface.

(ii) The three-step model including an isotropic photoexcitation process for the description of the volume photoeffect.

(iii) The linear relation between the surface photoeffect and the squared amplitude of the E_z field component normal to the emitting surface.

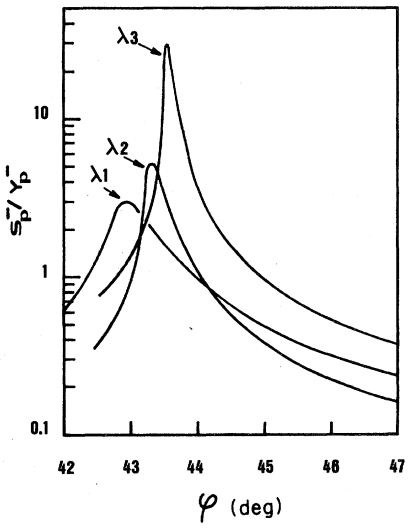

FIG. 19. Variation of the ratio S_p^-/Y_p^- as a function of φ, for three values of the photon wavelength. ($\lambda_1 = 350$, $\lambda_2 = 500$, $\lambda_3 = 765$ nm), SPW being excited in the film.

(iv) The possibility of adding both effects to find a correct value for the total emission, implying that no interference of any kind exists between surface and volume effect in our polycrystalline metal film.

(v) The utilization, in our photon energy domain situated far below the surface plasmon energy $\hbar\omega_s$ of Al, of the metal classical optical constants, corresponding to a local description of the dielectric constant.

To our knowledge no quantitative interpretation of photoemission, even in free-electron-like metals has hitherto been successful in the photon energy domain well below the surface plasmon energy. At higher energies, in the region of surface and volume plasmons, only approximate values of the surface effect have been obtained[51,52] in experiments on Al clean surfaces directly illuminated by synchrotron radiation. More accurate values of the surface-effect contribution have been recently reported for indium smooth thin film[53] in the photon energy range $6 < \hbar\omega < 10.5$ eV located just below the volume plasmon energy of In.

Many reasons may be invoked to explain the discrepancies observed by other authors together with the good agreement existing in our results between theoretical and experimental values of the spectral sensitivity in the presence of an SPW which still profoundly disturbs the energy distribution in the film, a situation very different from the simple case of a direct illumination of the metal surface.

(i) Perfectly smooth surfaces are imperative to ensure a total absence of surface photoeffect in s-polarized illumination in order to determine an accurate value of the volume photoeffect contribution.

(ii) The electronic properties of the surface, and most particularly the work function, must remain stable for periods of time long enough to perform the series of measurements for obtaining improved accuracy. Such a stability is obtained for Al-Cs surfaces only in a very good UHV, with a residual pressure less than 5×10^{-11} Torr.

(iii) All calculations are based upon the knowledge of the true optical constants of the metal film. The thickness and the complex permittivity of each film have to be measured *in situ*, the latter being always slightly different from the optical constants values which are found in the literature.

Our study of photoemission from Al surfaces near the threshold energy, lowered by a submonolayer of Cs atoms evaporated on the surface, indicates that volume- and surface-effect contributions are both strongly enhanced by excitation of a surface plasma wave, but that the angular varia-

tions of the emission currents originating in these two distinct photoexcitation mechanisms are profoundly different. The volume and surface photoemission peaks correspond, respectively, to two distinct angles of incidence φ, which are both different from the angle which makes the reflecting power of the film a minimum, these phenomena being well explained by the angular variations of the absorbed energy repartitions in the film. Near the emission threshold, the surface photoeffect exceeds the volume photoeffect by a factor of almost 10, in agreement with the theoretical values given by Endriz,[12] and we have shown that SPW excitation enhances the surface effect more than the volume effect. Another important point deserves comment: Slightly varying the angle of incidence beyond φ_L gives the possibility of dramatically changing the ratio of surface effect to volume effect at constant wavelength (Fig. 19). Such experimental facility would certainly be useful in photoelectron spectroscopy for the study of surface states.

ACKNOWLEDGMENTS

This work was supported by the Centre National de la Recherche Scientifique under Contract No. ATP 2449. The author would like to express his deep gratitude to Professor A. Septier, who initiated this work, for many stimulating discussions and critical reading of the manuscript. Useful discussions with Professor G. A. Boutry and Professor P. Lebon are also gratefully acknowledged.

[1]W. E. Spicer, Phys. Rev. 112, 114 (1958).
[2]C. N. Berglund and W. E. Spicer, Phys. Rev. 136, A1030 (1964).
[3]J. G. Endriz, and W. E. Spicer, Phys. Rev. B 4, 4159 (1971).
[4]G. Hincelin and A. Septier, J. Phys. (Paris) Lett. 41, 127 (1980).
[5]G. D. Mahan, Phys. Rev. B 2, 4334 (1970).
[6]P. J. Feibelman and D. E. Eastman, Phys. Rev. B 10, 4932 (1974).
[7]J. K. Sass, Surf. Sci. 51, 199 (1975).
[8]S. A. Flodstrom, G. V. Hansson, S. B. M. Hagstrom, and J. G. Endriz, Surf. Sci. 53, 156 (1975).
[9]S. V. Pepper, J. Opt. Soc. Am. 60, 805 (1970).
[10]G. Chabrier, J. P. Goudonnet, and P. J. Vernier, Phys. Rev. B 13, 4396 (1975).
[11]I. Tamm and S. Schubin, Z. Phys. 68, 97 (1931).
[12]J. G. Endriz, Phys. Rev. B 7, 3464 (1973).
[13]P. J. Feibelman, Phys. Rev. Lett. 34, 1092 (1975).
[14]G. D. Mahan, Phys. Rev. B 2, 4334 (1970).
[15]W. L. Schaich and N. W. Ashcroft, Phys. Rev. B 3, 2452 (1971).
[16]C. Caroll, D. Lederer-Rozenblatt, B. Roulet, and D. Saint-James, Phys. Rev. B 8, 4552 (1973).
[17]K. L. Kliewer and R. Fuchs, Phys. Rev. 172, 607 (1968).
[18]K. L. Kliewer, Phys. Rev. B 14, 1412 (1976).
[19]A. R. Melnyk and M. J. Harrison, Phys. Rev. B 2, 835 (1970).
[20]G. Chabrier, Ph.D. thesis, Dijon University, 1978 (unpublished).
[21]G. Chabrier, J. P. Goudonnet, and P. J. Vernier, Opt. Commun. 29, 178 (1979).
[22]A. Otto, Z. Phys. 216, 398 (1968).
[23]E. Kretschmann and H. Raether, Z. Naturforsch A 23, 2135 (1968).
[24]H. Kanter, Phys. Rev. B 1, 522 (1970).
[25]T. Kloos, Z. Phys. 265, (1973).
[26]J. Crowell and R. H. Ritchie, J. Opt. Soc. Am. 60, 794 (1970).
[27]E. Kretschmann, Z. Phys. 227, 412 (1971).
[28]R. H. Ritchie, Surf. Sci. 34, 1 (1973).
[29]J. G. Endriz and W. E. Spicer, Phys. Rev. B 4, 4144 (1971).
[30]S. N. Jasperson and S. E. Schnatterly, Phys. Rev. 188, 759 (1969).
[31]E. Kretschmann, Opt. Commun. 10, 353 (1974).
[32]K. L. Hornauer, Opt. Commun. 16, 76 (1976).
[33]C. F. Eagen and W. H. Weber, Phys. Rev. B 19, 5068 (1979).
[34]J. C. Dudek and G. Hincelin, C. R. Acad. Sci. 286, 257 (1978).
[35]E. Krestchmann, Z. Phys. 241, 313 (1971).
[36]J. Bösenberg, Z. Phys. B 22, 261 (1975).
[37]J. Bösenberg, Phys. Lett. 37A, 439 (1971).
[38]C. S. Wang, J. Appl. Phys. 48, 1477 (1978).
[39]T. A. Calcott and A. U. MacRae, Phys. Rev. 178, 966 (1969).
[40]J. J. Uebbing and L. W. James, J. Appl. Phys. 41, 4505 (1970).
[41]P. M. Cungry, R. Holton, and V. Leverett, Surf. Sci. 43, 647 (1974).
[42]H. J. Clemens, J. Von Wienskowski, and W. Monch, Surf. Sci. 78, 648 (1978).
[43]J. Monin and G. A. Boutry, Phys. Rev. B 9, 1309 (1974).
[44]T. E. Fisher, Phys. Rev. 142, 519 (1966).
[45]G. Hincelin and A. Septier, in *Proceedings of the 7th International Vacuum Congress and Third International Conference on Solid Surfaces, Vienna, 1977*, edited by R. Dobrozemsky, F. Rüdenauer, F. P. Viehböck, and A. Breth (F. Berger and Söhne, Vienna, 1977), p. 1269.
[46]A. G. Mathewson and H. P. Myers, Phys. Scr. 4, 291 (1972).
[47]J. Kadlec, Phys. Rep. 26C, 69 (1976).
[48]Theoretical expressions for the quantum yield Q may be found in Ref. 9 and E. Coquet and P. J. Vernier, C. R. Acad. Sci. 262 Serie B, 1141 (1966).
[49]T. A. Calcott and E. T. Arakawa, Phys. Rev. 11, 2750 (1975).
[50]G. Chabrier, J. P. Goudonnet, and P. J. Vernier, Phys. Rev. B 13, 4396 (1976).
[51]H. Petersen and S. B. M. Hagström, Phys. Rev. Lett. 41, 1314 (1978).
[52]H. Petersen, Z. Phys. B 31, 171 (1978).
[53]G. Jezequel, Phys. Rev. Lett. 45, 1963 (1980).